PHYSICAL REVIEW D **80,** 024012 (2009)

Perturbed disks get shocked: Binary black hole merger effects on accretion disks

Miguel Megevand,[1] Matthew Anderson,[2] Juhan Frank,[1] Eric W. Hirschmann,[3] Luis Lehner,[1] Steven L. Liebling,[4] Patrick M. Motl,[5] and David Neilsen[3]

[1]*Department of Physics and Astronomy, Louisiana State University, Baton Rouge, Louisiana 70803-4001, USA*
[2]*Department of Mathematics, Brigham Young University, Provo, Utah 84602, USA*
[3]*Department of Physics and Astronomy, Brigham Young University, Provo, Utah 84602, USA*
[4]*Department of Physics, Long Island University–C.W. Post Campus, Brookville, New York 11548, USA*
[5]*Department of Natural, Information and Mathematical Sciences, Indiana University Kokomo, Kokomo, Indiana 46904, USA*
(Received 22 May 2009; published 14 July 2009)

The merger process of a binary black hole system can have a strong impact on a circumbinary disk. In the present work we study the effect of both central mass reduction (due to the energy loss through gravitational waves) and a possible black hole recoil (due to asymmetric emission of gravitational radiation). For the mass reduction case and recoil directed along the disk's angular momentum, oscillations are induced in the disk which then modulate the internal energy and bremsstrahlung luminosities. On the other hand, when the recoil direction has a component orthogonal to the disk's angular momentum, the disk's dynamics are strongly impacted, giving rise to relativistic shocks. The shock heating leaves its signature in our proxies for radiation, the total internal energy and bremsstrahlung luminosity. Interestingly, for cases where the kick velocity is below the smallest orbital velocity in the disk (a likely scenario in real active galactic nuclei), we observe a common, characteristic pattern in the internal energy of the disk. Variations in kick velocity simply provide a phase offset in the characteristic pattern implying that observations of such a signature could yield a measure of the kick velocity through electromagnetic signals alone.

DOI: 10.1103/PhysRevD.80.024012 PACS numbers: 04.25.D−, 04.25.dk, 04.30.Db, 95.85.Sz

I. INTRODUCTION

The study of a number of astrophysical systems will soon add gravitational wave astronomy as a new tool to complement observations in the electromagnetic band. Since most systems capable of producing detectable gravitational waves will also radiate strongly in the electromagnetic band (see, e.g., [1,2]), combining information from both spectra will allow for a richer description of these systems. Furthermore, the complementary nature of observation in both bands will help the detection enterprise as a signal in one band will help follow up studies in the other (see, for instance, [3,4].)

Among interesting possible sources of strong signals in both spectra, the collision of a binary black hole system within a circumbinary disk presents the possibility of a detection of gravitational waves (as the black holes merge), which will be followed by electromagnetic signals emitted by the disk as its dynamics are affected in the process [5]. This scenario is common in nature, since massive black holes exist in the core of most galaxies and galaxies undergo mergers throughout their evolutionary path. As galaxies merge, they produce a binary black hole in the newly formed galaxy which eventually collide as their orbit shrinks through several mechanisms. As discussed in [5], a circumbinary disk is formed as the binary hollows out the surrounding gas, and the disk becomes mostly disconnected from the binary's dynamics [6,7]. Afterwards, while the disk remains essentially frozen, the black holes' orbits continue to shrink until they merge.

The merger process gives rise, in particular, to two relevant effects that will perturb the disk (see, e.g., [5,8]). One is related to the final mass of the black hole, which is less than the initial total mass as the system radiates energy via gravitational waves.[1] The other one is a consequence of the radiation of linear momentum, which if asymmetric (as in the case of an unequal mass binary, or asymmetric individual angular momenta of the black holes), induces a nontrivial recoil on the nascent black hole. This recoil effect has been predicted before through perturbative analysis of Einstein equations [10,11], and recent numerical simulations implementing the equations in full show even higher recoil velocities are possible [12–21]. The largest recoil velocities found correspond to mass ratios close to 1 and spins lying anti-aligned on the orbital plane. In the case of quasicircular orbits, recoil velocities up to about 4000 km/s have been calculated [14]. However, most of the black hole collisions occurring in nature are expected to produce kicks of about 500 km/s or less, since larger kicks would occur only in the case of nearly equal masses [22].

As a result of both effects mentioned above, the fluid dynamics in the disk is modified and shocks may be induced. The shocks' energy can then heat the gas, which can produce electromagnetic flares. These flares are expected to occur later (a few months to years), and to last

[1]Possible observable consequences of this effect were first discussed in [9].

considerably longer (thousands to hundreds of thousands of years)[23–25], suggesting tantalizing prospects for LISA observations aiding and complementing the electromagnetic observational prospects of these systems. For the recoiling black hole case, prior studies, which employ simulations of collisionless particles in Keplerian orbits forming a flat (zero height) disk, predict emissions ranging from UV to x-rays [23,24] or in the infrared [25] if this radiation is assumed to be absorbed before leaving the disk and re-emitted. Since these studies employ a particle description of the fluid, they can not fully capture the development (and hence influence) of shocks, which must be estimated by detecting collisions between particles. A recent work [26] adopted a field description for the fluid and studied the impact of a mass reduction in a pseudo-Newtonian potential to account for an innermost stable circular orbit (ISCO) at $r = 6M$ (which corresponds to the ISCO of a nonspinning black hole, while this is a rather uncommon output [27–30] in the merger of two black holes, the spin value will play a relevant role mainly if accretion develops). Based on computations of bremsstrahlung luminosity, that work predicts a decrease in luminosity as the fluid orbits adjust to the reduced gravitational potential.

In this work we study the effects on the disk by also considering a perfect fluid but in our case we do so employing the fully relativistic hydrodynamic equations in a background space-time. Thus, we are able to examine effects of spin, mass reduction and accretion, and comment on the relevance of different processes. In particular, our studies indicate that a significant distortion of the disk develops as time progresses when the kick has a component perpendicular to the disk's axis and that qualitatively similar features are present in all these cases.

In Sec. II, we briefly review our formulation of the problem and numerical approach. Section III describes our initial configuration. We discuss the observed dynamics in the disk after the merger has taken place in Sec. IV, taking into consideration the effect of mass reduction and different recoil velocities. Section V concludes and offers some further considerations.

Unless otherwise specified, we use geometrized units, where $G = c = 1$, and sum over repeated indexes. Greek-letter indices range from 0 to 3.

II. OVERVIEW OF THE NUMERICAL APPROACH

We implement the general relativistic MHD equations using a high resolution shock capturing module described in [31,32]. We introduce however a slight modification of the hydrodynamic equations inside the horizon to improve the fluid's behavior close to the excision region. Given an equation of the form[2]

$$\dot{U} + F(U)' = S, \tag{1}$$

we modify it in order to include a damping term

$$\dot{U} + F(U)' = S - f(r)(\Delta x)^p (U - U_0), \tag{2}$$

where the function $f(r)$ decreases smoothly with r, from 100 at the excision region to zero at the event horizon (EH), and is zero for $r \geq r_{\rm EH}$, so that the exterior of the black hole (BH) is causally disconnected from the effect of this extra term. U_0 is set to zero or to the value of the atmosphere if the corresponding field has one. The coefficient $(\Delta x)^p$ ensures that the damping term converges to zero and will not modify the convergence rate as long as one chooses p to be greater than or equal to the order of convergence of the code. In this work we adopt $p = 4$.

These equations are implemented within the HAD computational infrastructure, which provides distributed Berger-Oliger style adaptive mesh refinement [33,34] with full subcycling in time, together with a novel treatment of artificial boundaries [35]. Because of the dynamics involved in this work, it is only necessary to use a fixed refinement hierarchy, covering with finer grids the (central) region containing the disk and black hole, and increasingly coarser grids in the outer regions in order to locate the boundaries far away at a low computational cost.

III. OVERVIEW OF THE PHYSICAL SETUP

To explore the effects of the black hole merger in the dynamics of the accretion disk, we concentrate, in particular, in the post-merger stage—when the main burst of gravitational radiation has passed through the disk and this has settled down to a quasistationary state.[3] To simulate a BH formed through the merger process and account for the main effects of mass loss or recoil, we either consider a reduction in the mass of the black hole by 5% or apply a boost to the BH in a given direction. In the latter case, it is easier to adopt the BH's rest frame and apply the boost to the fluid variables (in the opposite direction) describing the disk, which is represented by a stationary toroidal solution of the fluid equations in a Kerr background. Thus, starting with a stationary torus on a Kerr background, we perform a Lorentz boost with velocity $-\vec{v}_{\rm kick}$ on the disk. We employ this boost to transform the fluid's 4-velocity u^μ and magnetic field 4-vector b^μ when considering the recoil case.

The toroidal solutions are constructed following an approach similar to that in [38], adapted to the ingoing Kerr-Schild coordinates adopted in our studies, and with a different choice of specific angular momentum for the fluid for easier comparison with previous work in the absence of magnetic fields. While in the current work we do not simulate scenarios that include a magnetic field, we discuss

[2]For clarity we use here a simple expression to represent the fluid equations. See [31,32] for the full equations.

[3]Studies of possible premerger effects are presented in, e.g., [36,37].

the construction of initial data that allows for doing so for future reference. In our case, we adopt the more standard $l \equiv -u_\phi (u_t)^{-1} = \text{const}$ (see below) to allow for an easier comparison with previous work in the absence of magnetic fields. In particular, we verify that identical solutions to those of [39] are obtained if the magnetic field is set to zero. In what follows we review the main steps in this construction.

The stress-energy tensor for ideal MHD can be written as

$$T_{\mu\nu} = (\rho h + b^2) u_\mu u_\nu + (P + b^2/2) g_{\mu\nu} - b_\mu b_\nu, \quad (3)$$

where ρ, P, and u^μ are the fluid's density, pressure and 4-velocity, respectively, b^μ is the magnetic field 4-vector, and h is the specific enthalpy, defined as

$$\rho h = \rho(1 + \epsilon) + P, \quad (4)$$

where ϵ is the specific internal energy density.

For the construction of initial data, we work with cylindrical coordinates (t, r, ϕ, z) and make the assumption that the space-time is stationary and axially symmetric. We adopt coordinates adapted to these symmetries, so that only the t and ϕ components of u^μ and b^μ are nonzero.

The fluid equations are obtained from

$$\nabla_\mu T^\mu{}_\nu = 0, \quad (5)$$

together with the continuity equation $\nabla_\mu(\rho u^\mu) = 0$ (which is trivially satisfied under our assumptions). After some manipulation, Eq. (5) can be reduced to the integral equation

$$\int u^t u_\phi d\left(\frac{u^\phi}{u^t}\right) - \ln u^t + \int \frac{1}{h\rho} dP + \int \frac{1}{2\rho h D} d(b^2 D) = \text{const}, \quad (6)$$

where $D = |g_{tt} g_{\phi\phi} - g_{t\phi}^2|$. This equation can be integrated after imposing further conditions that fix relationships between the fluid variables as discussed below.

First, we fix a relationship between the velocity components. This can be accomplished by requiring that the specific angular momentum l satisfies

$$l \equiv -\frac{u_\phi}{u_t} = \text{const}. \quad (7)$$

Second, we assume an isentropic fluid, imposing $dh = \rho^{-1} dP$, which allows us to integrate one of the terms out. An equation of state that satisfies this condition is that of a polytrope

$$P = \kappa \rho^\Gamma. \quad (8)$$

In this case, the specific internal energy density can be calculated as

$$\epsilon = \frac{\kappa}{\Gamma - 1} \rho^{\Gamma - 1}. \quad (9)$$

We adopt this condition only to obtain the stationary solutions for initial data. The fluid's entropy will change after the kick and so we adopt, during the evolution, a Γ-law equation of state

$$P = (\Gamma - 1)\rho\epsilon, \quad (10)$$

with $\Gamma = 5/3$ considering the gas as being monoatomic.

Finally, we impose a convenient expression for b^2 in terms of other variables to integrate the last term

$$b^2 D = C(\rho h D)^q, \quad (11)$$

where C and $q > 1$ are arbitrary constants.

After integrating Eq. (6), we use (8) and (9) to eliminate ρ and ϵ and obtain an algebraic equation for P, of the form

$$F(P, g_{\mu\nu}, l, C, q) = F_0, \quad (12)$$

where F_0 is a constant of integration. This equation can be solved analytically in the absence of magnetic field ($b^2 = 0$), otherwise a straightforward numerical integration can be set up to obtain the solution. The boundary of the torus is determined by setting $P = 0$, obtaining an expression of the form

$$f(g_{\mu\nu}, l) = F_0, \quad (13)$$

which, through the dependence of $g_{\mu\nu}$ on the coordinates, is an implicit surface equation. Notice that it is independent of both C and q so that the location of the disk's boundary is independent of the magnetic field. The solutions obtained may be toroidal as well as spheroidal, depending on the values of l and F_0.

Once P is known, one can use once again Eqs. (8) and (9) to recover ρ and ϵ. The velocity u^μ is obtained from Eq. (7) together with the normalization condition $u^\mu u_\mu = -1$. Finally, the magnetic field b^μ is determined by Eq. (11) together with the relation $b^\mu u_\mu = 0$ (see [31]). The magnetic filed is always zero at the surface of the disk (from Eq. (11)), and one can control how rapidly it decays to zero with the parameter q, and its maximum magnitude with C.

As mentioned, when considering the recoiling case, the initial data for a disk is given a Lorentz boost with respect to the stationary system of the background black hole. A representative example of the toroidal configurations is shown in Fig. 1. Such configurations are then evolved on a computational domain given by $[-150M, 150M]$ in the x and y direction, and $[-100M, 100M]$ in the z direction (since the disk lies on the $x - y$ plane), with a fixed mesh refinement configuration having 3 levels of refinement. The code used in our studies has been previously tested and employed in a variety of stringent scenarios, e.g., [32,40,41]. For our specific application we have verified that in the absence of a kick or mass reduction the disk remains stationary during the evolution as expected. Additionally, we have verified convergence by comparing results obtained with three different resolutions in the case

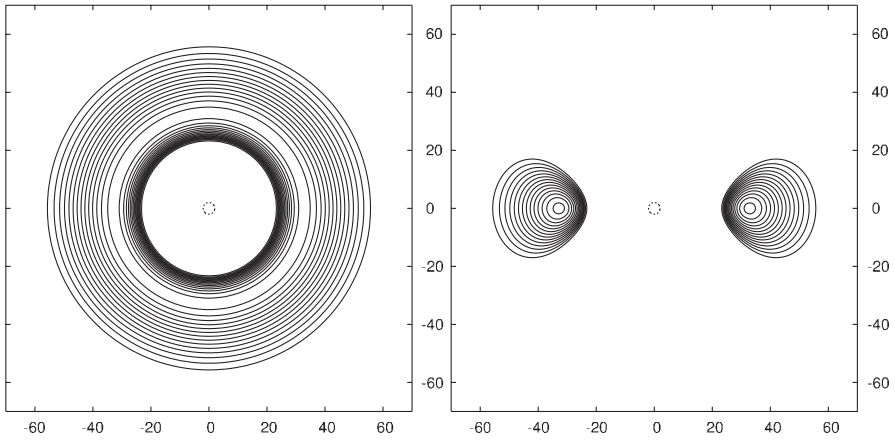

FIG. 1. Representative example of the toroidal initial configurations, showing the density at the equatorial plane (left panel), and at a meridional plane (right panel). The dashed line indicates the location of the event horizon.

of a kick velocity of 3000 km/s perpendicular to the axis of rotation. The convergence rate measured at different locations varies between first and third order depending on the presence of shocks.

Certainly the parameter space is too vast to allow an exhaustive computational study. Therefore, we mainly concentrate here on varying the most relevant parameters, i.e., the kick magnitude and direction and study a few other cases varying the spin parameter to verify our results are qualitatively the same. Notice that variations with respect to the spin parameter a should not lead to significant qualitative differences unless accretion develops, as the disk's inner edge is located sufficiently far away for its influence to be of higher order. This intuitive observation is confirmed by our simulations.

The toroidal solutions employed in this work correspond to specific angular momentum $l/M = 6$, spin parameter $a/M = 0.5$ (except when analyzing the solution's dependence on the spin where we also consider $a/M = 0.9$). Also, we fix the magnetic field parameter $C = 0$ (so that $b = 0$), and choose F_0 so that the inner edge of the disk is located at $r_{\rm in} = 20M$. With this choice of parameters, the outer edge is located at $r_{\rm out} = 60M$ and the maximum pressure in the disk lies at $r_{\rm m} = 33M$. The orbital velocity of the fluid is then 0.28, 0.17 and $0.10c$ at $r_{\rm in}$, $r_{\rm m}$, and $r_{\rm out}$, respectively. Thus, the orbital period at $r_{\rm m}$ is $P_{\rm m} = 1220M$. The sound speed has a maximum value $\lesssim 0.05c$ close to $r_{\rm m}$, and drops abruptly to zero at the boundary of the torus. All fluid elements in the torus have an orbital speed much greater than the highest kick velocity adopted in this work, i.e., $0.01c = 3000$ km/s and so will remain bound to the black hole in all cases considered.[4] In fact, the binding energy per unit mass at the surface of the torus is $0.0121c^2$, which implies an escape velocity of $0.155c$. Notice that the location of the disk's inner radius can vary significantly depending on diverse physical parameters (e.g., kinematic viscosity of the gas, accretion rate, binary mass ratio, etc.) [5]. We adopt a small value but within the allowed ones to reduce the computational cost of the long simulations required and concentrate on extracting physically robust conclusions, which can be intuitively extended to general cases.

Throughout the rest of this paper, unless otherwise specified, all kick orientations mentioned refer to the kick (or Lorentz boost) applied to the disk, which would correspond to the black hole being kicked in the opposite direction.

IV. RESULTS

A. Diagnostic quantities

We monitor the fluid's behavior by examining the dependence of the primitive values as different physical parameters are varied. Ultimately, our goal is to understand possible electromagnetic signals emitted by the system as the disk's dynamics is affected. At present, our simulations do not incorporate radiation transport; thus, a direct computation of these signals is not possible. Therefore, we concentrate on related quantities, which when combined with a suitable model, can be tied to possible emissions. In particular, we compute (an approximation to the) temperature (T), the total internal energy (U) and bremsstrahlung luminosity (L_B) as

$$T \propto P/\rho, \tag{14}$$

$$U \propto \int \rho \epsilon dV, \tag{15}$$

$$L_B \propto \int \rho^2 T^{1/2} dV. \tag{16}$$

Notice that unless the disk is optically thin, the bremsstrahlung luminosity need not capture the luminosity resulting

[4]For comparison purposes we have also employed the unrealistic value of 9000 km/s

from shocks and shock heating. While the bremsstrahlung luminosity is a good measure of the energy exchanged between atoms and the radiation field, it does not take into account how this energy can be radiated out of the disk. In the absence of a more refined model, the qualitative features of the true radiative behavior can be estimated simply by a black body assumption. We thus monitor the internal energy for this purpose and also the bremsstrahlung luminosity to obtain a measure of the mentioned energy exchange (as well as to make contact with results presented in [26]).

B. Axisymmetric cases: Black hole mass loss and kick along disk's angular momentum

As a first step we consider the effect of BH mass loss and that of a kick along the disk's orbital angular momentum. The former entails solely decreasing the mass of the black hole, while for the latter the mass is unchanged but a kick is introduced along the z axis. In both cases, the underlying axisymmetry of the problem is not broken, which as we shall see later, is a key issue.

For the mass loss case, we employ a toroidal solution corresponding to a black hole of mass M_0 for the initial data, and set $M = 0.95M_0$. The dynamics of the disk with either a reduced mass or a kick along the z axis behave in a rather smooth manner. For the mass reduced case, radial oscillations are induced as the different fluid elements follow their corresponding epicycles. For the case with a recoil velocity, further oscillations are generated by induced motions in the z axis as illustrated in Fig. 2. Indeed, the recoil motion of the black hole introduces a time-dependent vertical component of the black hole's gravitational pull on the disk. Using Newtonian mechanics for simplicity and ignoring pressure forces, one can show that a particle on a circular orbit with velocity $v_{\rm orb}$, after a vertical kick of magnitude $v_{\rm kick}$ only reaches a height $z = \sqrt{2}R(v_{\rm kick}/v_{\rm orb})$ above the original plane before turning around. Since $v_{\rm kick}$ is the same for all disk radii, the vertical displacement is minimal at $r_{\rm in}$ and maximal at $r_{\rm out}$. This results in a flexing axisymmetric mode, with the outer edge flopping about the most. This is supported by Fig. 2 if one defines the ''midplane'' of the disk by joining points at which the contours are vertical. This argument ignores pressure, but pressure gradients are unlikely to be very important away from shocks, and the behavior is qualitatively the same. Because all particles on a given radial annulus are kicked simultaneously, they remain in phase with each other and the flexing mode is naturally excited.

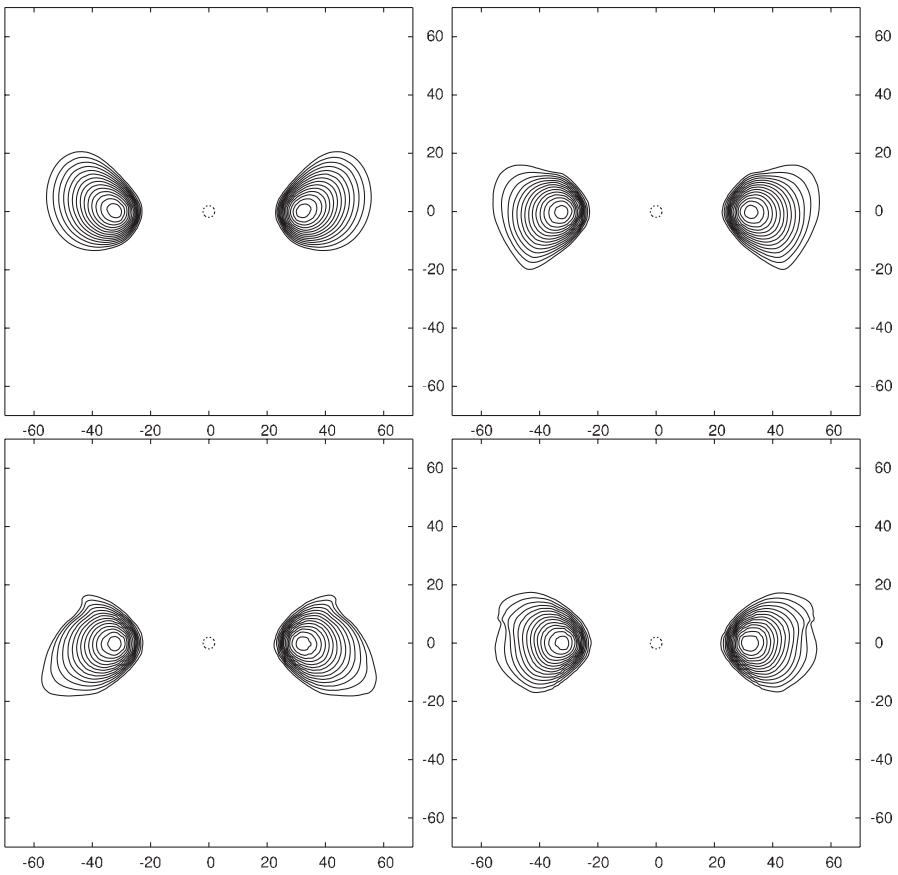

FIG. 2. Density at plane $y = 0$ in the case of a disk kicked with a velocity 3000 km/s in the positive z direction. The panels show snaps from $t/M = 500$ (top left) to 2000 (bottom right) at $\Delta t/M = 500$ intervals.

Note that maximum compression occurs twice per orbital period so this flexing mode is visible in both internal energy and bremsstrahlung at a frequency of about twice the orbital (See Figs. 3 and 4).

Most importantly, in either case no significant shocks are developed during the time of these simulations ($\simeq 6P_{\rm m}$). The observed smooth behavior translates into a rather monotonic behavior in our diagnostic variables. Figures 3 and 4 illustrate the internal energy and bremsstrahlung luminosity, respectively. The behavior observed in the latter case is qualitatively similar to results shown in [26], i.e., an initial drop followed by a recovery in luminosity. Our simulations, which extend farther, indicate that this behavior continues quasiperiodically. Notice however that the disk geometry considered in [26] is different from ours and the bremsstrahlung computed includes the inner portion of the disk while we do so for the complete disk. Last, the small drift observed in Fig. 3 is consistent with a linear accumulation of numerical error. A similar linear drift is observed in simulations of an unperturbed disk. This growth however is small—within 5%—over the length of the simulations considered ($\simeq 6P_{\rm m}$) and significantly smaller than the effects induced by the perturbations due to the recoiling black hole.

C. Asymmetric cases: kick with component orthogonal to disk's angular momentum

Next we concentrate on the oblique recoil case. For concreteness we adopt recoil velocity values $v_{\rm kick} = 300$, 1000 and 3000 km/s (we also consider 9000 km/s to verify the appearance of the main feature and check the empirical law presented below). We begin by examining the case where the kick direction is on the orbital plane (i.e., orthogonal to the angular momentum of the disk). The

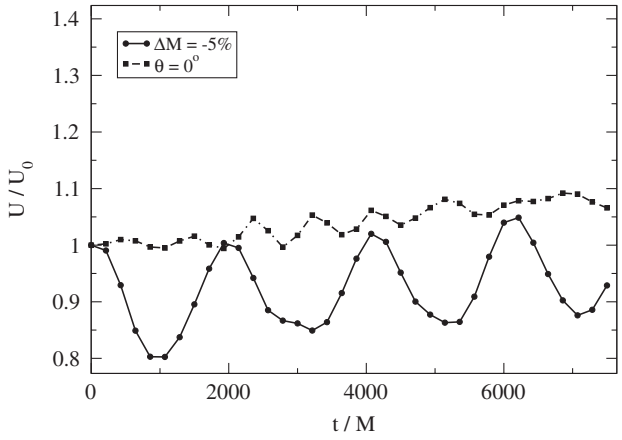

FIG. 3. Total internal (normalized) energy of the disk. The continuous line corresponds to a BH mass loss of 5% and no kick, while the dashed line corresponds to a kick with velocity $v_{\rm k} = 3000$ km/s along the axis of rotation (and no BH mass loss). The vertical scale and range was chosen to coincide with those in the other energy plots in this work for easy comparison.

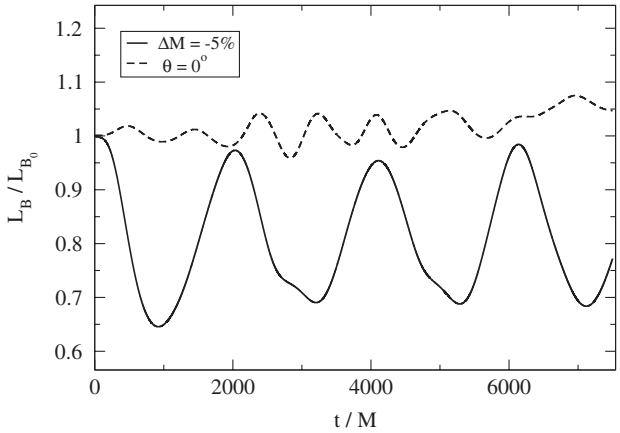

FIG. 4. Bremsstrahlung luminosity (normalized) of the disk. The continuous line corresponds to a BH mass loss of 5% and no kick, while the dashed line corresponds to a kick with velocity $v_{\rm k} = 3000$ km/s along the axis of rotation (and no BH mass loss).

simulations for the different cases proceed along qualitatively similar phases, which are illustrated for the case of $v_{\rm kick} = 3000$ km/s in Fig. 5 for ρ at $z = 0$, and in Fig. 6 for $|\nabla P|$ at $z = 0$. The asymmetry introduced by the kick's direction induces an accumulation of gas at one side of the disk, while causing a significant decrease on the opposite side. As time progresses, shocks develop and a complex dynamic arises, at late times $\simeq 6000M$, an accretion phase is clearly noticeable for $v_{\rm kick} > 1000$ km/s (see Fig. 7).

To analyze the impact of the disk dynamics and possible observable features, we compute the internal energy (Fig. 9) and bremsstrahlung luminosity (Fig. 10) for $v_{\rm kick} = 300$, 1000, and 3000 km/s. An initial relatively small bump is observed, which takes place at a time given by half the orbital period of the maximum density region, which is consistent with the epicyclic picture. From there on, a complex behavior is observed, though notably, irrespective of the magnitude of the kick, the same qualitative features are observed—especially in Fig. 9. Generally, we see that both the internal energy and the bremsstrahlung luminosity dip and rebound but the internal energy ends up higher, while the bremsstrahlung luminosity finishes lower. This can be understood as follows: the kick energy is dissipated in shocks, increasing the temperature and the pressure but the subsequent expansion reduces the density below the initial values. Because the bremsstrahlung emissivity is $\propto \rho^2 T^{1/2}$, the net effect is a reduction in emissivity despite the increase in pressure. The relative changes in both internal energy and bremsstrahlung luminosity are relatively modest, at a level of ~20–40% and occur on characteristic timescales on the order of $1000M = 5000M_6$ s, where M_6 is the mass of the black hole in $10^6 M_\odot$.

Second, we examine the dependence on kicks at different angles. Since the main qualitative features of all kick cases considered are similar, we concentrate in the case

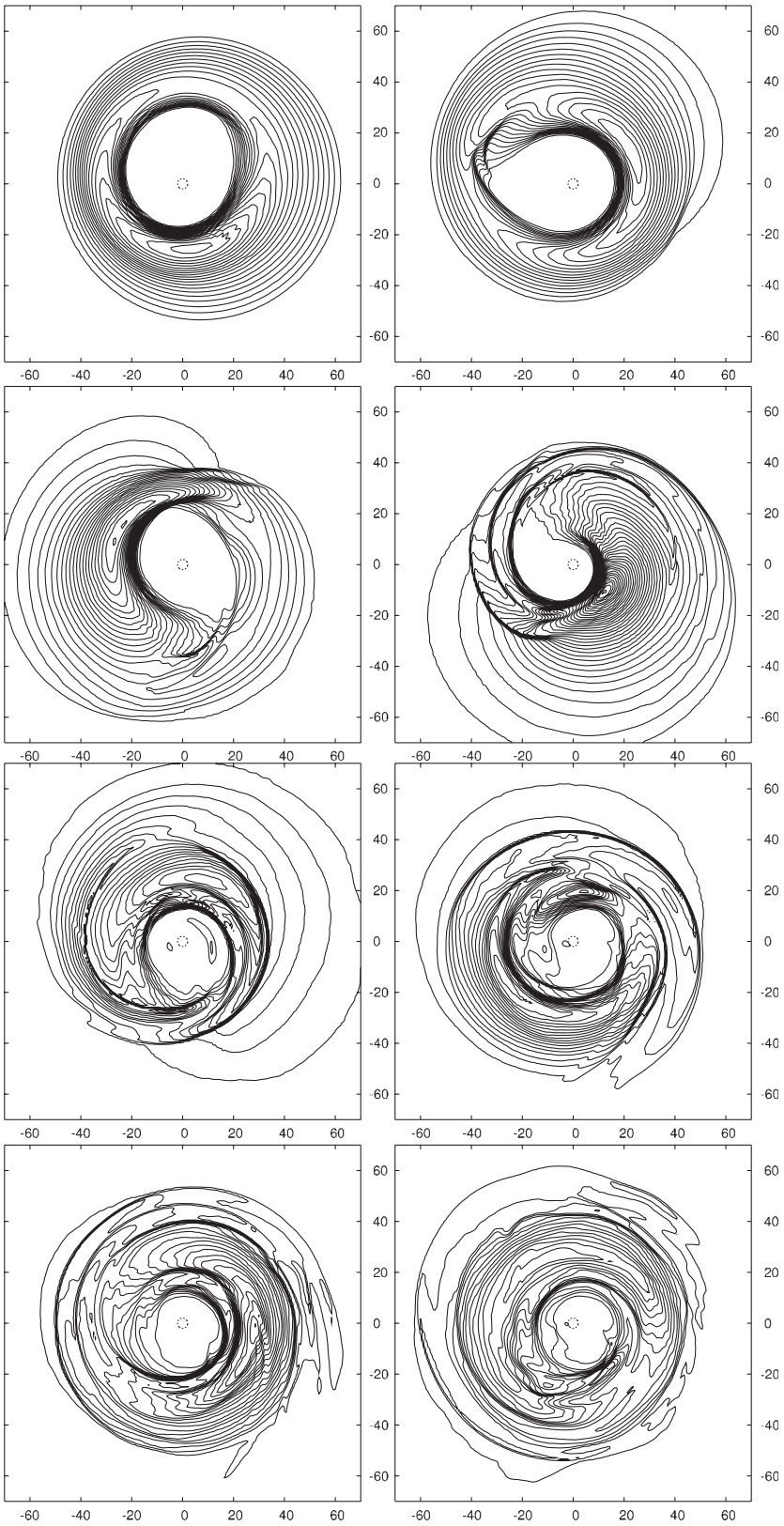

FIG. 5. Density ρ at plane $z = 0$ in the case of a disk kicked with a velocity 3000 km/s in the positive x direction, i.e., to the right of this page (which corresponds to the black hole being kicked to the left). The panels show snaps from $t/M = 500$ (top left) to 4000 (bottom right) at $\Delta t/M = 500$ intervals.

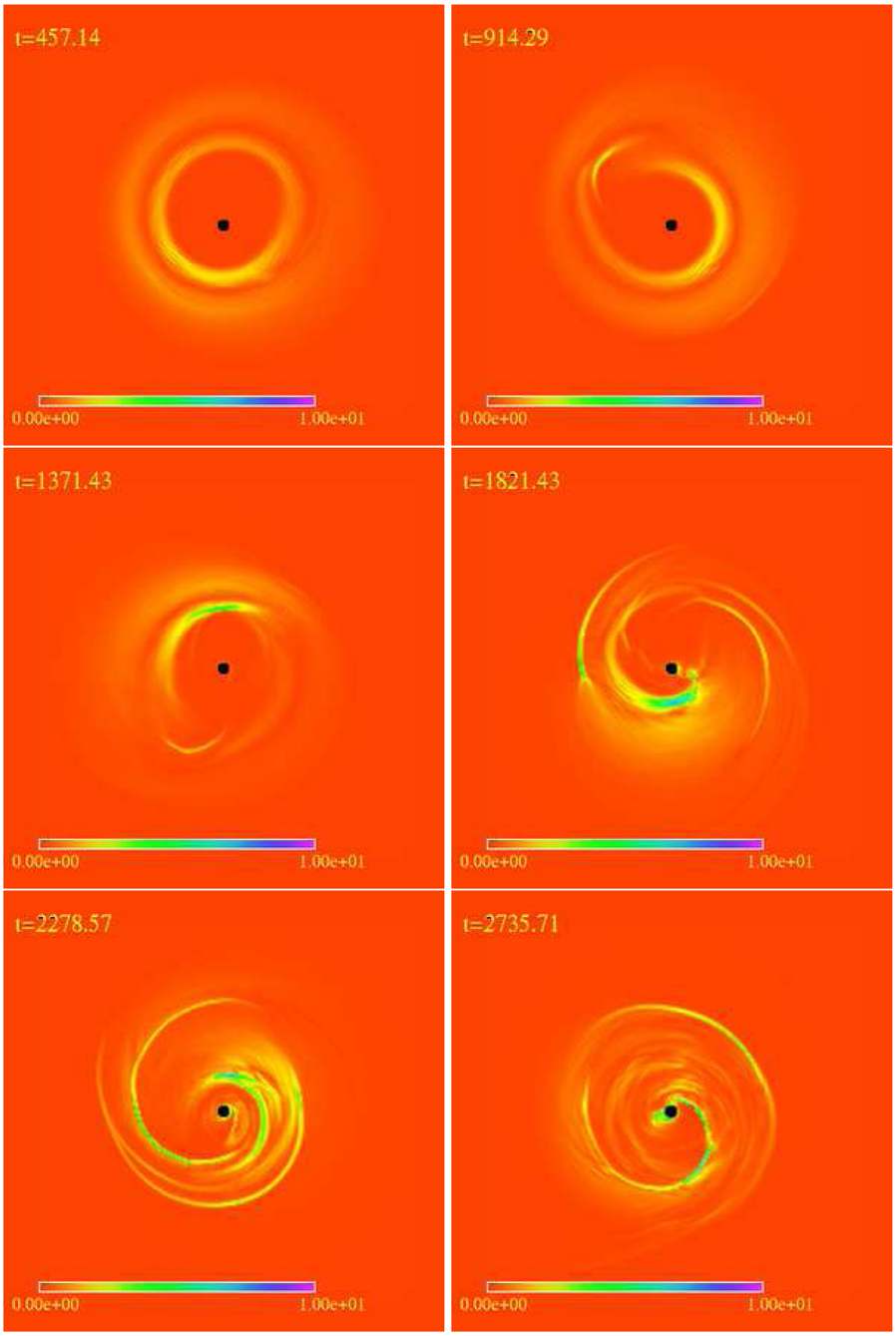

FIG. 6 (color online). To illustrate the formation of shocks we show here $|\vec{\nabla}P|$ at $z = 0$. Kick velocity of 3000 km/s in the positive x direction.

$v_{\rm kick} = 3000$ km/s as this is the one that displays the overall behavior within the shortest computational time. We compute the internal energy and bremsstrahlung luminosity for kicks at $\theta = 0$, 30, 60, and 90°, where the angle θ is measured with respect to the axis of rotation. Figure 11 shows the density at plane $z = 0$ in the case of a kick at 30°. Figures 8 and 12 illustrate the (normalized) internal energy and bremsstrahlung luminosity vs time for the different angles considered. Recall that no significant shocks form when the kick is along the axis of the disk. When the kick has a component along the disk's plane however, the qualitative features observed in the internal energy are similar for all cases. We note that the evolution we observe for a given $v_\perp = (3000 \text{ km/s}) \sin\theta$ is nicely bracketed by evolutions with pure orbital plane kicks above and below $v_\perp$. Thus, $v_\perp$ is the most important parameter determining the behavior of the kicked disk, apart from the small oscillations also present when the

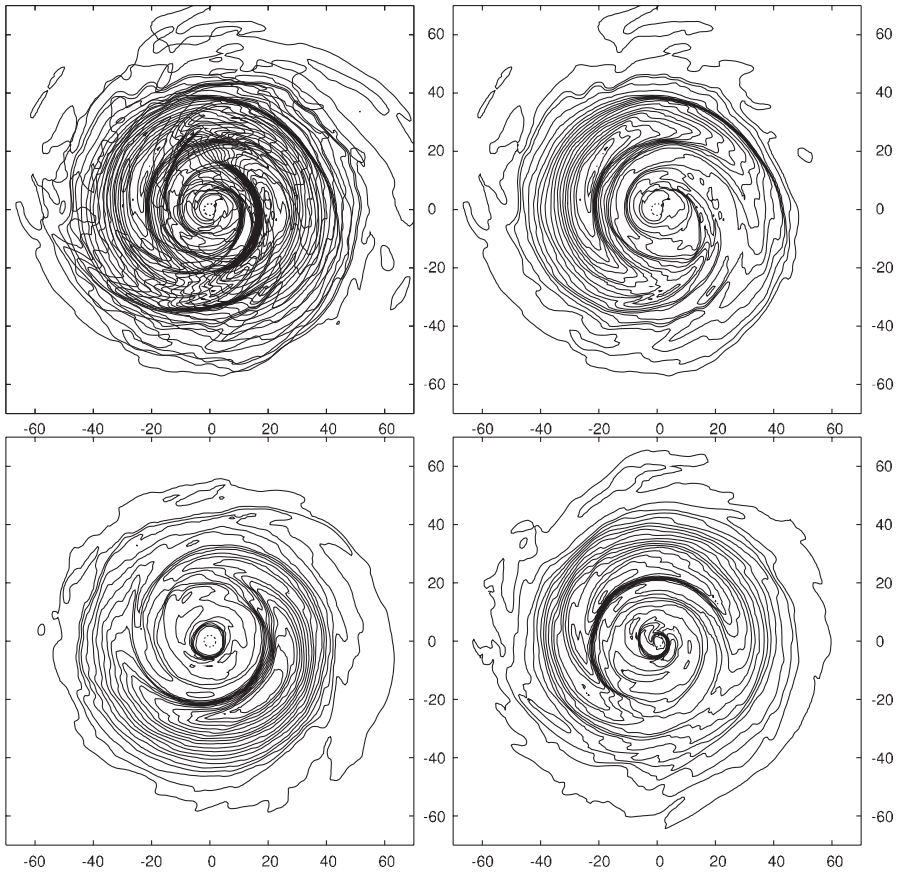

FIG. 7. Later stages of the simulation shown in Fig. 5, in which the gas begins to accrete into the black hole. The panels show snaps from $t/M = 6000$ (top left) to 7500 (bottom right) at $\Delta t/M = 500$ intervals. Notice that at $t/M = 7000$ the ISCO is clearly noticeable.

kick is parallel to the axis of rotation, and the likely small differences in the shape of the initial shock.

Another feature common to all the internal energy (or pressure) results (See Figs. 9 and 11) is a rapid swing from a dip to a bump, followed by an oscillating growth at a moderate pace. While the magnitude of the upward swing of the internal energy does not depend strongly on $v_\perp$, the time at which it occurs does. The delay we observe decreases as $v_\perp$ is increased. If this delay were due to the time taken by a perturbation traveling at $v_\perp$ to cross some fixed distance, one would expect a dependence $\propto v_\perp^{-1}$. Instead, we observe a logarithmic decrease. Defining the delay as the time after the initial kick at which the internal energy swings upward through the initial value, we find the following empirical dependence:

$$\frac{t_{\rm swing}}{M} = 5200 - 912 \ln\left(\frac{v_\perp}{300\ {\rm km/s}}\right). \qquad (17)$$

Note that this formula applied naïvely "predicts" an infinite delay for a kick along the axis of rotation.

As is well known, constant specific angular momentum tori are prone to a nonaxisymmetric corotation instability [42,43] whose nonlinear development has been explored numerically in the pseudo-Newtonian approximation [44] and in general relativistic magnetohydrodynamics [45]. The final outcome depends on the aspect ratio of the torus, the nature and strength of any large-scale magnetic fields present, the presence of accretion [46], and this remains to be fully investigated in the general relativistic magnetohydrodynamics context. Therefore, any substantial perpendicular component of the kick is likely to excite at some level the $m = 1$ nonaxisymmetric mode, which is expected to grow at a rate $\omega \approx 0.2\Omega_{\rm m}$, where $\Omega_{\rm m} = 2\pi/P_{\rm m}$ is the Keplerian angular frequency at the pressure maximum. For the parameters of the torus of our simulations $P_{\rm m} = 1220M$, and $\Omega_{\rm m} = 0.00515$. The behavior described above is suggestive: if one assumes that the initial pressure perturbation is $\delta P_0 \propto v_\perp^2$, which is reasonable for shocks and on dimensional grounds, and one sets $\delta P = \delta P_0 \exp\omega t$, then the time required for the perturbation to attain a given fiducial level would follow an equation of the form (17), with $t = t_{\rm ref} - (2/\omega)\ln(v_\perp/v_{\rm ref})$, where $t_{\rm ref}$ and $v_{\rm ref}$ are some arbitrary reference values. Analyzing the results we obtained indicates that $\omega = 0.43\Omega_{\rm m}$, which is on the order of the expected frequency but significantly higher. Thus, we suggest tentatively that the swing we see in both the

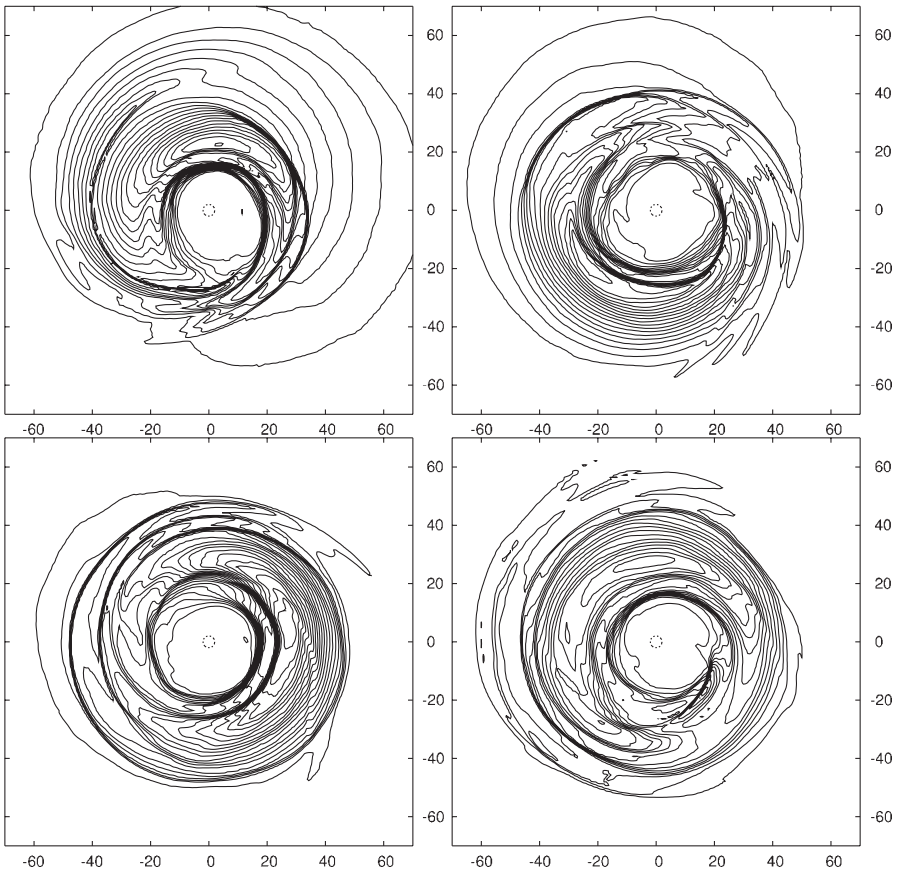

FIG. 8. Density ρ at plane $z = 0$ in the case of a disk kicked with a velocity 3000 km/s at $\theta = 30°$. The panels show snaps from $t/M = 2500$ (top left) to 4000 (bottom right) at $\Delta t/M = 500$ intervals.

internal energy and bremsstrahlung plots in all cases where there is a nonzero $v_\perp$ is a common transient response to the kick that may be observable in principle, and that the subsequent growth may be due to the growth of the instability and/or the rise to the expected level of dissipation of the input kinetic energy. At late times for the higher kicks our simulations display an accretion phase and so this possible saturation can not be explored, though a suggestive behavior consistent with this saturation is displayed by the largest kick considered.

We note that a similar swing in the bremsstrahlung luminosity was observed in the (axisymmetry preserving)

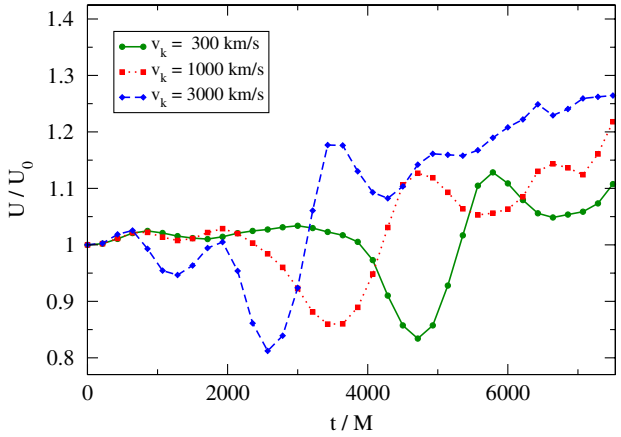

FIG. 9 (color online). Normalized internal energy. Kicks perpendicular to axis of rotation ($\theta = 90°$).

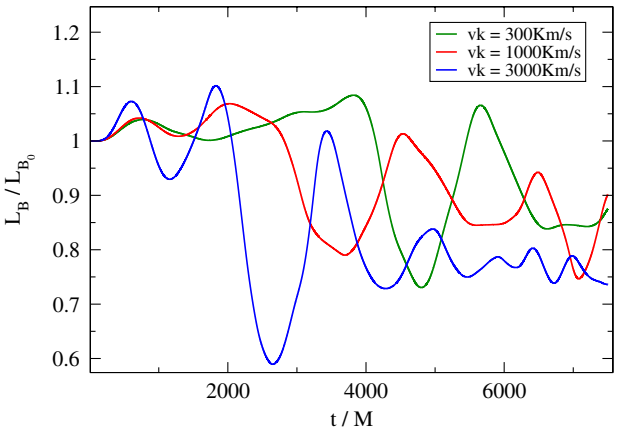

FIG. 10 (color online). Normalized bremsstrahlung luminosity. Kicks perpendicular to axis of rotation ($\theta = 90°$).

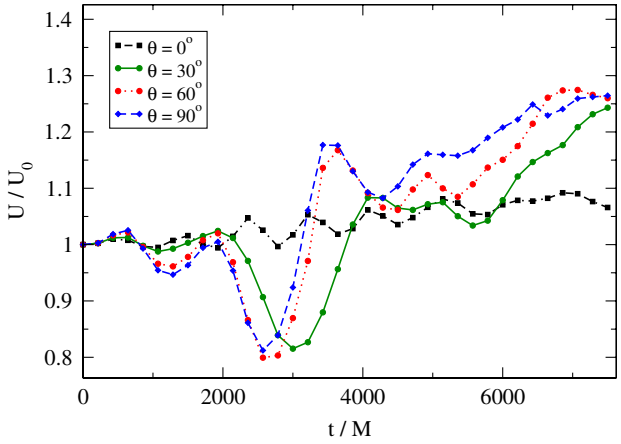

FIG. 11 (color online). Internal energy. Kicks at varying inclinations θ with respect to the axis of rotation. All cases with $v_{\rm kick} = 3000$ km/s.

simulations by O'Neill *et al.* [26] using thin disks, which are not prone to the Papaloizou and Pringle instability. In the near future, to further elucidate the relative importance of the transient response and the instability, we are planning an investigation of the effects of kicks in tori with flatter rotation laws $\Omega \propto r^{-q}$ since the aforementioned instability does not occur if $q < \sqrt{3}$ as well as examining magnetized tori.

D. Dependence on black hole spin

Finally, we investigate possible differences between cases with different black hole spins by performing a simulation with spin $a/M = 0.9$ in addition to the value $a/M = 0.5$ used in the rest of the simulations. For this test we chose the setting with kick velocity of 3000 km/s perpendicular to the disk's axis. Notice that although all other parameters coincide in these simulations, the stationary disk solutions used to construct the initial data

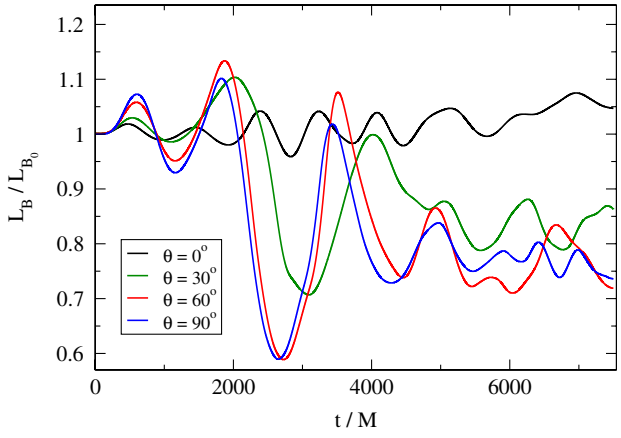

FIG. 12 (color online). Bremsstrahlung luminosity for kicks at varying inclinations θ with respect to the axis of rotation. All cases with $v_{\rm kick} = 3000$ km/s.

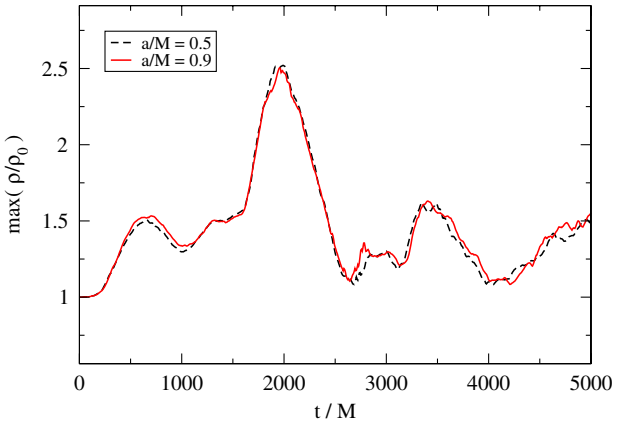

FIG. 13 (color online). Comparison of the maximum of density for black hole spins $a/M = 0.5$ (dashed line) and 0.9 (continuous line) for a kick of 3000 km/s perpendicular to the disk's axis.

are slightly different since they depend on a. Still, we see no significant differences, as is illustrated in Fig. 13, where we show a comparison between the maxima of density, normalized by dividing by its value at $t = 0$, which is slightly different in each case.

V. CONCLUSION

In the current work we have studied the possibility that binary black hole mergers, within a circumbinary disk, give rise to scenarios likely to emit electromagnetic radiation. We have studied both the impact of mass loss in the system and recoil velocities. While both induce deformations of the disk, it is the case of a recoiling black hole, when the recoil's direction has a component along the disk plane, that appears as the most promising option to generate an observable, electromagnetic, signature. This is so not just because the effect is larger, but also the variability induced is significantly more pronounced than that observed in the case of mass loss or kick along the disk's angular momentum. Furthermore, we find that the magnitude of the kick is not very important as long as it is less than the smallest orbital speed of the fluid. While the kick magnitude impacts the time at which the strongest variation in internal energy or bremsstrahlung appears, the intensity and time scale of the variation and behavior afterwards is not. Since supermassive binary black hole mergers will generically give rise to recoils (simply by having a mass ratio different from unity), which in turn ensures a kick component orthogonal to the final black hole spin, effects like those observed here indicate a possible a common behavior for the majority of scenarios.

Our studies also indicate that the final black hole spin has no strong effect on the main features of the solution. However, if an accretion phase takes place, the location of the innermost stable circular orbit will naturally play a key role.

ACKNOWLEDGMENTS

We would like to thank P. Chang, B. Kocsis, J. McKinney, C. Miller, S. Phinney, and J. Tohline for stimulating discussions. This work was supported by the NSF Grant Nos. PHY-0803629, PHY-0653375 and NASA ATP Grant No. NNX07AG84G to LSU, Contract Nos. PHY-0803615 and CCF-0832966 to BYU, and Contract Nos. PHY-0803624 and CCF-0833090 to LIU. Computations were done at BYU (Marylou4), the Louisiana Optical Network Initiative (LONI), LSU, and TeraGrid. L. L acknowledges the Aspen Center for Physics for hospitality where this work was started.

[1] J. Sylvestre, Astrophys. J. **591**, 1152 (2003).
[2] C. W. Stubbs, Classical Quantum Gravity **25**, 184033 (2008).
[3] Z. Haiman, B. Kocsis, K. Menou, Z. Lippai, and Z. Frei, Classical Quantum Gravity **26**, 094032 (2009).
[4] J. S. Bloom *et al.*, arXiv:0902.1527.
[5] M. Milosavljevic and E. S. Phinney, Astrophys. J. **622**, L93 (2005).
[6] P. J. Armitage and P. Natarajan, Astrophys. J. Lett. **567**, L9 (2002).
[7] F. K. Liu, X.-B. Wu, and S. L. Cao, Mon. Not. R. Astron. Soc. **340**, 411 (2003).
[8] B. Kocsis and A. Loeb, Phys. Rev. Lett. **101**, 041101 (2008).
[9] N. Bode and S. Phinney, APS Meeting Abstracts (2007).
[10] J. D. Bekenstein, Astrophys. J. **183**, 657 (1973).
[11] M. J. Fitchett, Mon. Not. R. Astron. Soc. **203**, 1049 (1983).
[12] J. G. Baker, W. D. Boggs, J. Centrella, B. J. Kelly, S. T. McWilliams, M. C. Miller, and J. R. van Meter, Astrophys. J. **668**, 1140 (2007).
[13] J. G. Baker, W. D. Boggs, J. Centrella, B. J. Kelly, S. T. McWilliams, M. C. Miller, and J. R. van Meter, Astrophys. J. Lett. **682**, L29 (2008).
[14] M. Campanelli, C. Lousto, Y. Zlochower, and D. Merritt, Astrophys. J. Lett. **659**, L5 (2007).
[15] M. Campanelli, C. O. Lousto, Y. Zlochower, and D. Merritt, Phys. Rev. Lett. **98**, 231102 (2007).
[16] J. A. González, U. Sperhake, B. Brügmann, M. Hannam, and S. Husa, Phys. Rev. Lett. **98**, 091101 (2007).
[17] J. A. González, M. Hannam, U. Sperhake, B. Brügmann, and S. Husa, Phys. Rev. Lett. **98**, 231101 (2007).
[18] F. Herrmann, I. Hinder, D. Shoemaker, and P. Laguna, Classical Quantum Gravity **24**, S33 (2007).
[19] F. Herrmann, I. Hinder, D. Shoemaker, P. Laguna, and R. A. Matzner, Astrophys. J. **661**, 430 (2007).
[20] W. Tichy and P. Marronetti, Phys. Rev. D **76**, 061502 (2007).
[21] J. G. Baker, J. Centrella, D.-I. Choi, M. Koppitz, J. R. van Meter, and M. C. Miller, Astrophys. J. Lett. **653**, L93 (2006).
[22] J. D. Schnittman and A. Buonanno, Astrophys. J. Lett. **662**, L63 (2007).
[23] G. A. Shields and E. W. Bonning, Astrophys. J. **682**, 758 (2008).
[24] Z. Lippai, Z. Frei, and Z. Haiman, Astrophys. J. Lett. **676**, L5 (2008).
[25] J. D. Schnittman and J. H. Krolik, Astrophys. J. **684**, 835 (2008).
[26] S. M. O'Neill, M. C. Miller, T. Bogdanovic, C. S. Reynolds, and J. Schnittman, arXiv:0812.4874.
[27] A. Buonanno, L. E. Kidder, and L. Lehner, Phys. Rev. D **77**, 026004 (2008).
[28] L. Boyle and M. Kesden, Phys. Rev. D **78**, 024017 (2008).
[29] L. Rezzolla *et al.*, Phys. Rev. D **78**, 044002 (2008).
[30] C. O. Lousto, M. Campanelli, and Y. Zlochower, arXiv:0904.3541.
[31] D. Neilsen, E. W. Hirschmann, and R. S. Millward, Classical Quantum Gravity **23**, S505 (2006).
[32] M. Anderson, E. W. Hirschmann, S. L. Liebling, and D. Neilsen, Classical Quantum Gravity **23**, 6503 (2006).
[33] http://www.had.liu.edu/.
[34] S. L. Liebling, Phys. Rev. D **66**, 041703 (2002).
[35] L. Lehner, S. L. Liebling, and O. Reula, Classical Quantum Gravity **23**, S421 (2006).
[36] C. Palenzuela, M. Anderson, L. Lehner, S. L. Liebling, and D. Neilsen, arXiv:0905.1121.
[37] P. Chang, L. Strubbe, K. Menou, and E. Quataert (private communication).
[38] M. Shibata, Phys. Rev. D **76**, 064035 (2007).
[39] M. Abramowicz, M. Jaroszynski, and M. Sikora, Astron. Astrophys. **63**, 221 (1978).
[40] M. Anderson, E. W. Hirschmann, L. Lehner, S. L. Liebling, P. Motl, D. Neilsen, C. Palenzuela, and J. E. Tohline, Phys. Rev. D **77**, 024006 (2008).
[41] M. Anderson *et al.*, Phys. Rev. Lett. **100**, 191101 (2008).
[42] J. C. B. Papaloizou and J. E. Pringle, Mon. Not. R. Astron. Soc. **208**, 721 (1984).
[43] P. Goldreich, J. Goodman, and R. Narayan, Mon. Not. R. Astron. Soc. **221**, 339 (1986).
[44] J. F. Hawley, Astrophys. J. **528**, 462 (2000).
[45] J.-P. De Villiers and J. F. Hawley, Astrophys. J. **589**, 458 (2003).
[46] O. M. Blaes, Mon. Not. R. Astron. Soc. **227**, 975 (1987).